Available online at www.sciencedirect.com
ScienceDirect
Journal of Catalysis 248 (2007) 268–276
JOURNAL OF CATALYSIS
www.elsevier.com/locate/jcat

Photocatalysis of dicarboxylic acids over TiO_2: An in situ ATR-IR study

Igor Dolamic, Thomas Bürgi *

Institut de Microtechnique, Université de Neuchâtel, Rue Emile-Argand 11, 2009 Neuchâtel, Switzerland

Received 9 January 2007; revised 5 March 2007; accepted 22 March 2007

Available online 27 April 2007

Abstract

Attenuated total reflection infrared (ATR-IR) spectroscopy in a flow-through cell was used to study the photocatalytic mineralization of malonic acid and succinic acid over P25 TiO_2 in situ. The experiments were performed in water at concentrations of 1.5×10^{-4} mol/L and pH 3.5 at room temperature. Changes on the catalyst surface were observed within a few minutes. The first step in the mineralization of malonic acid is a photo-Kolbe reaction of adsorbed malonate. Part of the resulting C_2 species is converted into oxalate and finally into carbon dioxide, and part desorbs from the surface. The branching ratio for the two pathways is 50:50. The mineralization reaction was also observed in the absence of dissolved oxygen, but at a slower rate. In the presence of dissolved $^{18}O_2$, labeled oxygen was incorporated into the adsorbed oxalate. A dominant pathway in the mineralization of succinic acid involves the transformation to oxalate via malonate. Thus, it is proposed that a favored pathway for dicarboxylic acid mineralization is a photo-Kolbe reaction, followed by oxidation of the carbon-centered radical to a carboxylate, which corresponds to the overall formal shortening of the alkyl chain by one CH_2 unit.

Keywords: In situ spectroscopy; Photocatalysis; Attenuated total reflection; TiO_2, Malonic acid

1. Introduction

The ecologically and economically driven demand for sustainable technologies has fostered interest in methods for abatement of pollutants in wastewater. Photocatalysis over TiO_2 has great advantages in this important field [1–3]. TiO_2 is nontoxic and inert, and sunlight can be used to excite the semiconductor across its band gap. This process generates an electron–hole pair. Oxidation is assumed to proceed via direct attack of adsorbed species on the catalytic surface by photogenerated holes or to be indirectly mediated by radicals, such as $^{\cdot}OH$, generated from adsorbed water, oxygen, and hydroxyl groups on the catalyst surface. In this way, hazardous organic compounds can be completely mineralized, that is, converted into water and carbon dioxide.

Much data are available on the disappearance of organic molecules from the liquid phase during illumination of the photocatalyst and the evolution of dissolved intermediate species on the way to complete mineralization [3–5]. The nature of the catalytic interface during illumination has been explored much less extensively. Analyzing the processes occurring at the catalytic interface is perhaps the most direct way to unravel the mechanism of heterogeneous catalytic reactions. Attenuated total reflection infrared (ATR-IR) spectroscopy [6] is an ideal tool for investigating solid–liquid interfaces of powders [7,8]; it recently has been applied to study heterogeneous catalytic reactions occurring at solid–liquid interfaces [9–16]. Although applications of ATR-IR to photocatalysis are still limited [17–25], the technique's potential has been demonstrated.

Modulation excitation spectroscopy [26] was recently combined with ATR-IR to study heterogeneous catalytic reactions. The catalytic system is perturbed by periodically modulating an external parameter [10]. A subsequent phase-sensitive detection selectively highlights the species affected by the modulated parameter and also leads to a significant increase in sensitivity. Up to now, concentration modulation experiments in a flow-through cell (i.e., periodically varying the concentration of one

* Corresponding author. Fax: +41 32 718 25 11.
E-mail address: thomas.burgi@unine.ch (T. Bürgi).

0021-9517/$ – see front matter
doi:10.1016/j.jcat.2007.03.020

reactant at the inlet of the flow-through ATR-IR reactor) were used to disturb the catalytic system [10,27,28].

Here we also use light modulation to turn the photocatalytic reactions on and off, and we apply this strategy to study the photocatalytic mineralization of malonic acid and succinic acid over TiO_2 (P25). We have recently shown that oxalic acid is an important reaction intermediate on the TiO_2 surface in the mineralization of malonic acid [24]. The modulation technique also enables detection of the final reaction product, dissolved CO_2, near the interface. Selective ^{13}C labeling of malonic acid and ^{18}O labeling of dissolved oxygen gas gives additional information about the fate of malonic acid during mineralization. The phase-sensitive detection also provides evidence of the presence of carbonates on the TiO_2 surface during photocatalysis.

2. Experimental

2.1. Catalyst and chemicals

Degussa P25 TiO_2, containing 80% anatase and 20% rutile with a surface area of 51 m^2/g and average primary particle size of 21 nm, was used in the photocatalysis experiments. Malonic acid (Sigma-Aldrich, 99%), malonic-2-^{13}C acid (Aldrich, 99% ^{13}C), and succinic acid (Sigma-Aldrich, 99%) were used as received. Nitrogen (N_2, 99.995%), oxygen (O_2, 99.995%), and carbon dioxide (CO_2, 99.995%), all from CarbaGas, were applied to saturate the liquids. Labeled oxygen $^{18}O_2$ was received from Isotec (99%).

2.2. Thin-film preparation

A slurry of the catalyst powder was prepared from about 20 mg of catalyst and 25 mL of water (Milli-Q, 18 MΩ cm). After sonication (Branson 200 ultrasonic cleaner) for 30 min, TiO_2 thin films were formed by dropping the slurry onto a Ge internal reflection element (IRE) (52 × 20 × 1 mm; KOMLAS). In contrast to ZnSe, Ge was found to be inert under the applied experimental conditions. The amount of the slurry used for one coating was 0.5 mL. The solvent was allowed to evaporate, and the procedure was repeated twice. After drying for several minutes at 40 °C in air, loose catalyst particles were removed by flowing water over the IRE. After air-drying, the film was ready for use. From the amount of deposited TiO_2 and its density, an average film thickness of 4 μm was estimated. Fresh films were prepared every day, and results were reproducible on different catalyst films. It should also be noted that no adsorption and no reaction was observed in the absence of TiO_2 film.

2.3. In situ spectroscopy

ATR spectra were recorded with a dedicated flow-through cell composed of a Teflon piece and a fused silica plate (45 × 35 × 3 mm). The cell inlet was connected to two bubble tanks, allowing rapid exchange between two different fluids. The inlet–outlet distance was 36 mm. A flat (1 mm) viton seal defined the thickness of the fluid compartment, which had a volume of about 0.5 mL. The cell was mounted on an attachment for ATR measurements (Wilks Scientific) within the sample compartment of a Bruker Equinox-55 FTIR spectrometer equipped with a narrow-band MTC detector. Spectra were recorded at room temperature with a resolution of 4 cm^{-1}.

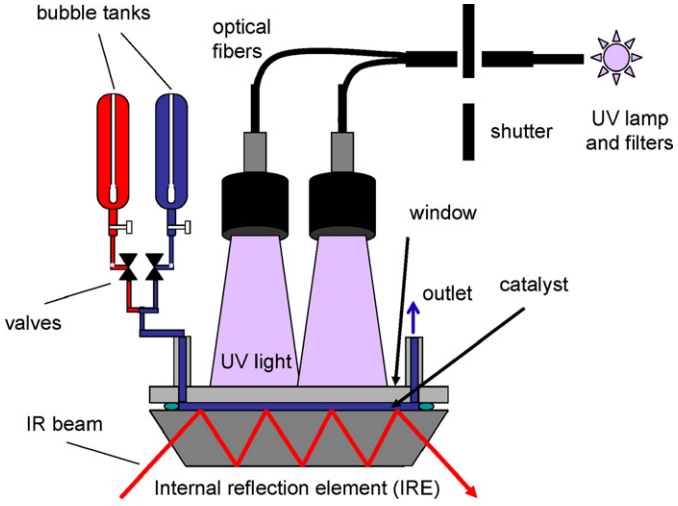

Fig. 1. Schematic setup for in situ ATR-IR spectroscopy of photocatalytic reactions in a small volume flow-through cell.

The solvent was saturated with gases in the two separate glass bubble tanks, then passed through the cell and over the sample by means of a peristaltic pump (Ismatec, Reglo 100) located after the cell. A flow rate of 0.2 mL/min was used. Unless stated otherwise, the solvent was saturated with air.

For irradiation of the sample, UV light was provided by a 75 W Xenon arc lamp. The UV light from the source was guided to the ATR-IR cell via two fiber bundles. The light was passed through a 5-cm water filter to remove any infrared radiation. A Schott UG 11 (50 × 50 × 1 mm) broadband filter from ITOS was used to remove visible light (transmission at 270–380 nm). An estimate based on the supplier specifications gave a power at the sample of slightly below 10 mW/cm^2. The experimental setup is shown schematically in Fig. 1.

2.4. Modulation experiments and data acquisition

The periodic variation of an external parameter has a specific influence on the catalytic system. The concentration of all of the species in the system affected by this external parameter will also change periodically at the same frequency as the stimulation. The following parameters were used for the modulation: the UV light flux, the reactant concentration (malonic acid) and the nature of the dissolved gas, oxygen–nitrogen. During one modulation period (typically 150–235 s), 60 IR spectra were recorded at a sampling rate of 40 or 80 kHz (4–8 scans/s) using the rapid scan function of the FTIR spectrometer. Typically 20 scans per spectrum recorded in a single period were averaged. Two modulation periods were performed before data acquisition was started. The IR spectra were than averaged over five modulation periods.

Modulation experiments were performed as follows. UV light modulation was achieved using an electronic shutter

(Newport model 71445). The light flux was modulated (on–off) in the presence of dissolved carboxylic acid or neat water over the TiO_2 catalyst.

For the gas modulation experiments, carboxylic acid solutions were saturated by nitrogen and oxygen in two separate glass bubble tanks. A nitrogen- or oxygen-saturated solution of the acid was than passed over the TiO_2 catalyst for 15 min. The modulation experiments were performed by switching two pneumatically actuated valves (Fig. 1).

The concentration modulation experiments used two glass tanks, one containing neat water (pH 5.5) and the other containing 1.5×10^{-4} mol/L carboxylic acid (pH 3.5). At this concentration, the dissolved acid was not observed in the ATR-IR spectra. Before the modulation experiments, the carboxylic acid solution was flowed over the sample for 30 min in the dark. At this point, the signals no longer changed, indicating equilibrium. At higher solution concentrations, the signals of the adsorbed species did not increase significantly, indicating saturation of the surface.

In all modulation experiments, data acquisition and modulation were synchronized. Electrical signals generated by the FTIR spectrometer within the data acquisition loop were used to switch the valves (concentration or gas modulation) or the shutter (light modulation). Note that the modulation experiments performed here are square wave modulations. Under certain conditions (e.g., during light exposure and in the dark), the demodulated spectra can be viewed as (high-quality) difference spectra between two states of the system. However, if different species in the system have different kinetics, then the spectra change qualitatively with demodulation phase angle. Modulation experiments are applicable only when the system response is reversible, which was verified by performing two or more identical modulation experiments one after the other.

The time-resolved absorbance spectra $A(\tilde{\nu}, t)$ were transformed into phase-resolved spectra using a digital phase sensitive detection (PSD) according to

$$A_k^{\phi_k^{\mathrm{PSD}}}(\tilde{\nu}) = \frac{2}{T}\int_0^T A(\tilde{\nu}, t)\sin\left(k\omega t + \phi_k^{\mathrm{PSD}}\right)\mathrm{d}t,$$

where $k = 1, 2, 3, \ldots$ determines the demodulation frequency (e.g., fundamental, first harmonic), T is the modulation period, $\tilde{\nu}$ denotes the wavenumber, ω the stimulation frequency, and ϕ_k^{PSD} is the demodulation phase angle. With a set of time-resolved spectra $A(\tilde{\nu}, t)$, the foregoing equation can be evaluated for different demodulation phase angles, ϕ_k^{PSD}, resulting in a series of phase-resolved spectra, $A_k^{\phi_k^{\mathrm{PSD}}}$. Only spectra demodulated at the fundamental frequency ($k = 1$) are reported here; more detailed information on the technique is available elsewhere [10,29].

3. Results and discussion

3.1. Major adsorbed species during illumination of adsorbed malonate

Fig. 2 shows ATR-IR spectra of (a) normal and (b) ^{13}C-labeled malonic acid adsorbed on the TiO_2 from aqueous air-saturated solution in the dark. Note that only the central carbon atom (C-2; Scheme 1) was ^{13}C-labeled. The most intense bands are assigned to carboxylate vibrations ν_{as}(COO) at 1625 and 1575 cm^{-1} and ν_s(COO) at 1436 and 1353 cm^{-1} [24]. As is evident from Fig. 2, ^{13}C labeling of the central carbon atom of malonic acid has no influence on these bands, which corroborates their assignment to the two terminal carboxylate groups. In contrast, the $\delta(CH_2)$ band at 1259 cm^{-1} shifts down to 1250 cm^{-1} on ^{13}C labeling. The spectra provide evidence

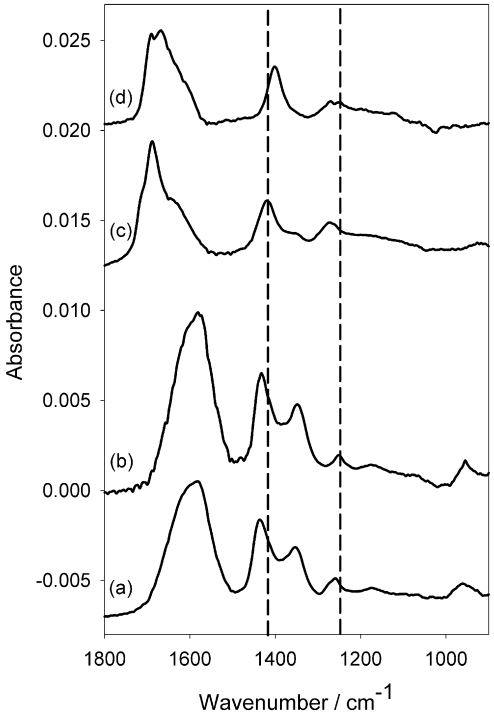

Fig. 2. ATR-IR spectra of (a) malonic acid and (b) ^{13}C-labeled malonic acid adsorbed from aqueous solution (1.5×10^{-4} mol/L) on TiO_2 in the dark and of the corresponding adsorbed reaction product ((c), unlabeled and (d) ^{13}C-labeled) after illumination for 7 min and flowing neat water for 14 min. Malonic acid was allowed to adsorb for 30 min before recording the spectra. Note that only the central C atom of malonic acid was labeled.

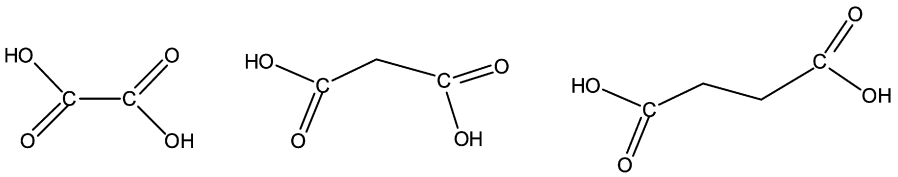

Oxalic acid Malonic acid Succinic acid

Scheme 1. Structure of oxalic, malonic and succinic acid.

for two largely different carboxylate groups consistent with one monodentate and one bidentate/chelating adsorption geometry [24].

Spectra (c) and (d) in Fig. 2 were obtained after illuminating adsorbed malonate and ^{13}C-labeled malonate, respectively, on TiO_2 in the presence of dissolved (labeled) malonic acid and oxygen and subsequent washing with water. The latter procedure, which removes adsorbed malonic acid within 14 min, leaves behind oxalate species formed on illumination [24]. The two spectra are clearly different; in particular, several bands associated with the COO vibrations shift to lower wavenumbers for oxalate formed from the ^{13}C-labeled malonate. The two bands of partly labeled oxalate at 1689 and 1669 cm^{-1} are the antisymmetric and symmetric combination of two C=O stretching vibrations, ν_s(C=O) and ν_{as}(C=O), respectively. The bands at 1401 and 1272 cm^{-1} are associated with ν(C–O) + ν(C–C) modes [30], whereas the band at 1249 cm^{-1} can be assigned to δ(O–^{13}C=O). This clearly shows that the central (labeled) carbon atom of the malonate ends up in the oxalate, as expected. Strongly adsorbed carboxylic acids are thought to undergo a photo-Kolbe reaction, initiated by a photogenerated hole, leading to CO_2 and a carbon-centered radical [31,32]. The latter ultimately leads to the oxalate. We have previously shown that oxalate adsorbed on TiO_2 is rapidly decomposed on illumination, leading to CO_2 [24].

3.2. Dissolved carbon dioxide

The enhanced sensitivity achieved by the phase-sensitive detection made the observation of dissolved CO_2 reaction product possible. Fig. 3 shows a demodulated spectrum of a light modulation experiment. In that experiment, a solution of ^{13}C-labeled malonic acid was flowed through the ATR-IR cell. The two bands at 2343 and 2277 cm^{-1} belong to dissolved CO_2 and $^{13}CO_2$ in water. These band positions are in good agreement with previous reports [33]. Note that due to the rotational envelope, gas-phase CO_2 has a distinctly different band shape from that shown in Fig. 3.

The first CO_2 molecule resulting from the photo-Kolbe reaction of selectively ^{13}C-labeled malonate, according to Scheme 2, is not labeled. Only in the further decomposition of the resulting C_2 compounds is one of the two CO_2 molecules ^{13}C-labeled. Complete mineralization of the selectively ^{13}C-labeled malonic acid leads to three CO_2 molecules, one of which is labeled, and hence to a $CO_2/^{13}CO_2$ ratio of 2.0. The intensity of the observed signals in Fig. 3 is clearly different from 2.0; in fact, the ratio of the corresponding integrated signals is 3.2. Keep in mind that the absorption coefficient of the asymmetric stretching vibration is affected by the isotopic labeling. A density functional theory (DFT) calculation reveals that the molar absorption coefficient ε is 5% lower for

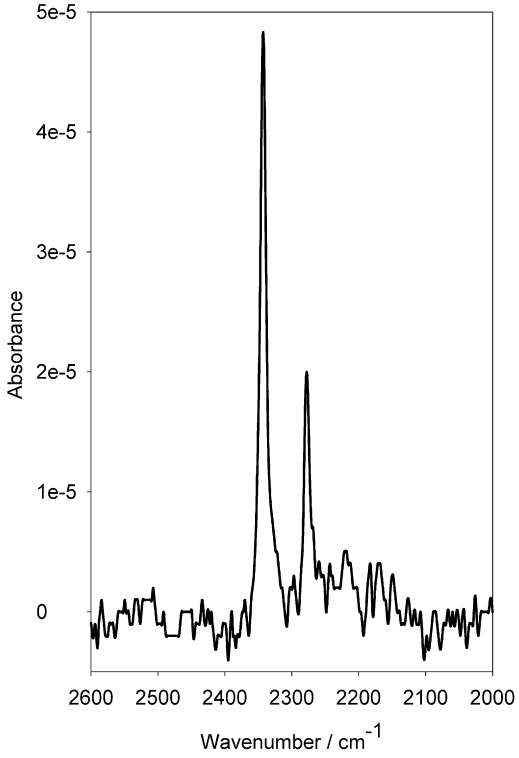

Fig. 3. Demodulated ATR-IR spectrum of a light modulation experiment where selectively ^{13}C-labeled malonic acid (1.5×10^{-4} mol/L) was flowed over the TiO_2 film. During one half of the modulation period ($T = 155$ s) the sample was illuminated and during the other half the sample was in the dark.

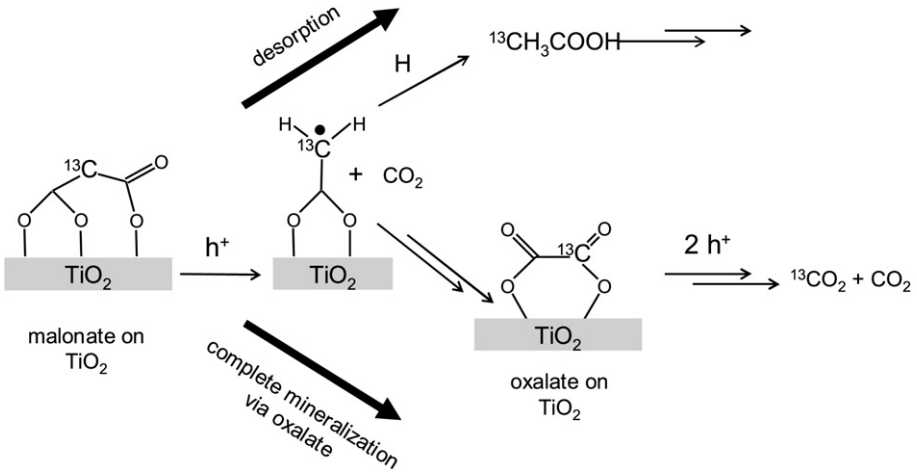

Scheme 2. Mechanism of photocatalytic mineralization of malonic acid over TiO_2.

labeled $^{13}CO_2$. According to $C_{CO_2}/C_{^{13}CO_2} = A_{CO_2}/A_{^{13}CO_2} \times \varepsilon_{^{13}CO_2}/\varepsilon_{CO_2}$, where C stands for the concentration and A for the integrated absorbance, a relative observed concentration of $3.2 \times 0.95 = 3.04$ is obtained. This demonstrates that part of the C_2 intermediate species formed during the initial photo-Kolbe reaction are desorbing from the surface and are washed away in the flow-through reactor before being further converted to CO_2.

The intermediates from the first photo-Kolbe reaction of malonic acid derive from a carbon-centered radical (Scheme 2). One of these intermediates, oxalate, is observed by ATR-IR. It has been shown that oxalate hardly desorbs from the TiO_2 (P25) surface and that it mineralizes rapidly under the present conditions [24], resulting in one labeled and one unlabeled CO_2 according to Scheme 2. Other intermediate species deriving from the carbon-centered radical may be acetic acid (by abstraction of a hydrogen) and glycolic acid (hydroxyacetic acid), which are not observed on the TiO_2 surface by ATR-IR. Acetic acid is known to adsorb only weakly [34] and thus desorbs from the catalyst surface before being further mineralized. Glycolic acid adsorbs more strongly on TiO_2 than acetic acid. There is no sign of it in the spectra [21], indicating that it is not formed. From the observed relative concentration of labeled and unlabeled CO_2, the branching ratio of C_2 intermediates that are converted into oxalic acid (and completely mineralized) and acetic acid or other C_2 species that are desorbing from the surface can be determined. The limiting cases result in $CO_2/^{13}CO_2$ ratios of 2.0 for complete mineralization (via oxalate) and infinity for no further mineralization of C_2 intermediates. The observed $CO_2/^{13}CO_2$ ratio of 3.0 corresponds to a fraction of 50% that is completely mineralized (mainly via oxalate, yielding one labeled and two unlabeled CO_2 molecules) and 50% that is desorbed and washed away as C_2 species before being mineralized (yielding one unlabeled CO_2 molecule). In this context, it is illustrative to mention the residence time in the flow-through reactor, which is about 2.5 min.

The concentrations of dissolved CO_2 observed while flowing a solution of 1.5×10^{-4} mol/L malonic acid over the TiO_2 film and during illumination can be quantified. To do so, the observed absorbance (5×10^{-5} at 2343 cm^{-1}) was compared to that measured while a solution saturated with CO_2 was flowed over the TiO_2 film (0.0136 at 2343 cm^{-1}). At 25 °C, about 0.035 mol/L of CO_2 can be dissolved in water [35]. Only a small fraction of the dissolved CO_2 (<1%) is converted to carbonic acid. Most of the CO_2 remains solvated molecular CO_2, giving rise to the signal at 2343 cm^{-1}. Thus, the observed absorbance signal of 0.0136 for a saturated CO_2 solution corresponds to a concentration of 0.035 mol/L, and the signal (5×10^{-5}) observed during the photocatalytic mineralization corresponds to a concentration of 0.035 mol/L $\times$ $(5 \times 10^{-5}/0.0136) = 1.29 \times 10^{-4}$ mol/L, compared with the 1.5×10^{-4} mol/L malonic acid in solution.

Fig. 4 shows the signal at 2343 cm^{-1} of CO_2 as a function of time during a light modulation experiment. Obviously, the time-dependent signal is quite noisy; nonetheless, useful information on mass transport out of the volume probed by the evanescent field can be obtained from this signal, assuming that CO_2 is produced only during illumination. When the light is shut off, the

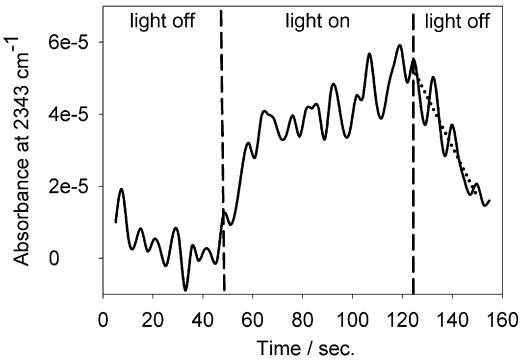

Fig. 4. Absorbance at 2343 cm^{-1} associated with CO_2 as a function of time during a light modulation experiment ($T = 155$ s, concentration of malonic acid: 1.5×10^{-4} mol/L). The dashed line was used for the calculation of the diffusion rate of CO_2 out of the catalyst film (see text).

CO_2 concentration decreases due to diffusion out of the evanescent field. The penetration depth of the latter is estimated to be 0.31 μm at 2343 cm^{-1}, as calculated from the refractive index of Ge (4.0) and the estimated effective refractive index (1.82) of the TiO_2 film in water. The latter is estimated from the refractive indices of water (1.33) and TiO_2 (2.2) by assuming a porosity of 0.5 according to $n_{\text{eff}} = (0.5(n_{H_2O})^2 + 0.5(n_{TiO_2})^2)^{1/2}$. Because the penetration depth is considerably less than the film thickness, the observed decrease of the CO_2 signal in the dark is dominated by internal diffusion within the TiO_2 film. During illumination in the steady state, the diffusion of CO_2 is compensated for by photocatalytic mineralization,

$$\frac{dc}{dt} = 0 = -\left(\frac{dc}{dt}\right)_{\text{diff}} + \left(\frac{dc}{dt}\right)_{\text{reaction}}.$$

In the dark, the term due to reaction vanishes, and the observed decrease of the signal corresponds to the diffusion. A rough estimate from Fig. 4 yields $(dc/dt)_{\text{diff}} = 3.4 \times 10^{-6}$ mol/(L s), which also corresponds to the estimated rate of production of CO_2 within the film during illumination. The reaction rate with respect to malonic acid is about half this value (1.7×10^{-6} mol/(L s)), taking into account the branching ratio discussed above and thus prompting the observation that on average, each reacting malonic acid molecule leads to two CO_2 molecules under our conditions.

3.3. Minor adsorbed species on TiO_2 during illumination

Carbonate species might be expected on the TiO_2 surface during the mineralization of malonic acid and oxalic acid, due to the presence of dissolved CO_2 and the observation that carbonate ions (HCO_3^-, CO_3^{2-}) strongly adsorb on metal oxides [36]. Furthermore, oxygen-rich compounds adsorbed on the surface during malonic acid mineralization could directly convert into carbonates. No carbonates have been observed by ATR-IR during the photocatalytic mineralization of oxalic acid [25] and glyoxylic acid [21], and the spectra shown in Fig. 2 reveal no obvious sign of such species; however, the presence of carbonates becomes obvious from modulation experiments. Fig. 5 (bottom) shows a demodulated spectrum for a malonic acid concentration modulation experiment. One advantage of

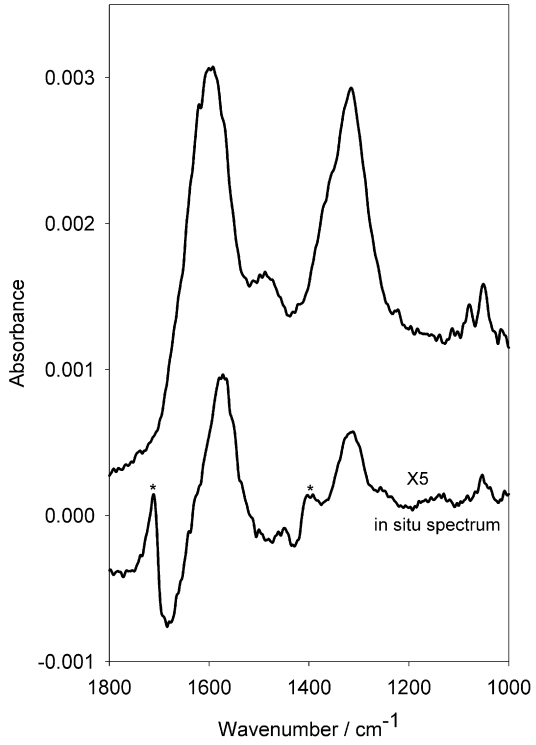

Fig. 5. Bottom: demodulated ATR-IR spectrum of a concentration modulation experiment ($T = 155$ s, concentration of malonic acid: 1.5×10^{-4} mol/L). The demodulation phase angle was chosen such that the signals of adsorbed malonate vanish. Bands marked with an asterisk are associated with oxalate. Top: ATR-IR spectrum of carbonate species on the TiO_2 surface. The spectrum was measured after flowing a saturated aqueous CO_2 solution over the sample followed by flowing water.

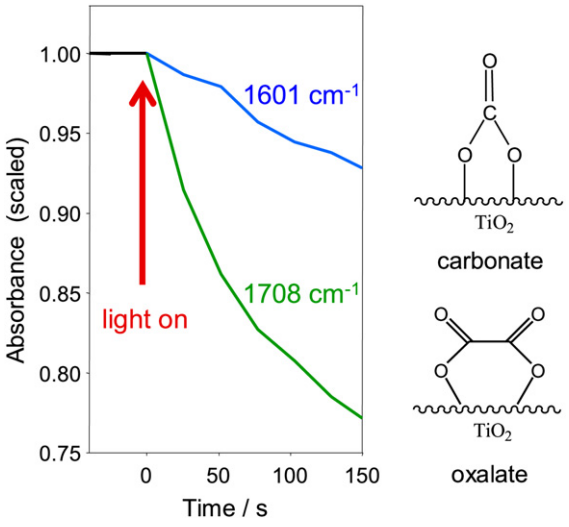

Fig. 6. ATR-IR signals of carbonate (1601 cm^{-1}) and oxalate (1708 cm^{-1}) as a function of time during illumination. The signals were obtained from two different experiments and the signal before starting illumination was scaled to one. The surface covered by the carbonates was obtained by flowing a saturated solution of CO_2 over the sample followed by a flow of water. The surface covered by the oxalate was obtained by flowing a malonic acid solution saturated with oxygen over the sample during illumination followed by a flow of water in the dark.

the digital phase-sensitive detection is that the demodulation phase angle can be chosen such that the dominant species is completely removed from the spectrum. In the present case, the demodulation phase angle ϕ_k^{PSD} was adjusted to 90° to remove the strong signals of adsorbed malonate, uncovering weaker signals of other species with different time (and thus also phase) behavior. For comparison, Fig. 5 (top) shows an ATR-IR spectrum obtained after flowing a saturated aqueous solution of CO_2 over the TiO_2 sample and after washing with water. This leads to the formation of carbonate species on the TiO_2 surface such as monodentate and bidentate carbonates, bicarbonate and also carboxylate [37]. Most importantly, the comparison in Fig. 5 clearly shows the presence of carbonates on the catalyst surface during the mineralization of malonic acid. The most prominent bands observed at 1598 and 1317 cm^{-1} can be assigned to bidentate carbonate and monodentate carbonate, respectively [37]. The positive bands in the demodulated spectrum marked with an asterisk belong to oxalate, which has a different time behavior than that of malonate; therefore, the oxalate signals do not vanish at the same demodulation phase angle as those of malonate. The sharp band at 1053 cm^{-1} is assigned to a C–O stretching vibration of a carbonate species. The negative band at 1680 cm^{-1} in the demodulated spectrum (partly overlapping with the carbonate band at 1598 cm^{-1}) may be assigned to bicarbonate species, which would mean that these bicarbonate species have different time (and phase) behavior than the other carbonates.

The carbonate species are stable in a flow of water at neutral pH in the dark; however, their concentration on the surface decreases on illumination in water. Desorption or decomposition may be initiated by capturing a photogenerated hole. Fig. 6 shows the decrease of the signals at 1601 and 1708 cm^{-1} associated with carbonate ions and oxalate species, respectively. The two signals measured before illumination were normalized to one absorbance unit. Note that the two curves were obtained from two separate experiments in which the two species, carbonates and oxalate, were selectively prepared on the surface before illumination. Clearly, carbonate species disappear considerably slower than oxalate.

The concentration of carbonate species on the TiO_2 surface is not large during illumination, and thus it is not observed in "normal" time-resolved experiments. The carbonate signals are about 10 times smaller in the demodulated spectrum than in the upper spectrum shown in Fig. 5, with the latter corresponding to a surface saturated with carbonates. Thus, the coverage of carbonates during illumination under our conditions is on the order of 10% of a full coverage. Nonetheless, the carbonates slow down the mineralization process due to competition for adsorption sites and for photogenerated holes. The comparison in Fig. 5 also shows that the relative intensity of the signals associated with monodentate and bidentate carbonate is different for the two experiments, indicating that the relative ratio of monodentate and bidentate carbonates differs when formed by adsorption of CO_2 on a clean TiO_2 surface and when formed during photocatalysis. This difference may be due to the blocking of specific sites by the malonate and oxalate species in the latter case.

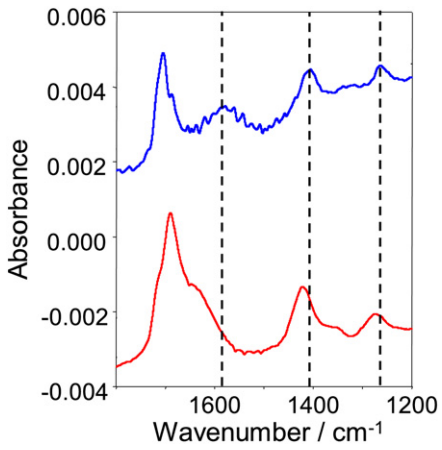

Fig. 7. ATR-IR spectra of oxalate on TiO_2. The spectra were obtained by flowing a malonic acid solution saturated with oxygen over the sample during illumination followed by a flow of water in the dark. For the bottom spectrum normal oxygen (O_2) was used. For the top spectrum labeled oxygen ($^{18}O_2$) was used. Vertical lines are used to guide the eye.

3.4. The role of oxygen

For the total mineralization of malonic acid according to

$$C_3H_4O_4 + 2O_2 \xrightarrow[TiO_2]{h\nu} 3CO_2 + 2H_2O,$$

oxygen must be provided. In this equation, this corresponds formally to two oxygen molecules, but the source of oxygen remains to be determined. Several possibilities are conceivable. The oxygen may come directly from dissolved O_2 molecules. In fact, previous reports on photocatalysis over TiO_2 proposed reactive oxygen species deriving from O_2 as important intermediates responsible for the oxidation of organic pollutants [3,38]. In an aqueous environment, the incorporated oxygen also may originate from water. For example, the carbon-centered radical may pick up OH from water. Finally, the TiO_2 surface may serve as an oxygen source. In this case, the oxygen consumed needs to be regenerated from either water or dissolved O_2. To shed some light on the role of oxygen, labeled $^{18}O_2$ was used, and modulation experiments were performed in which the dissolved gas, O_2 and N_2, served as the stimulation.

Fig. 7 shows ATR-IR spectra of oxalate. In these experiments, the TiO_2 sample was illuminated while solutions of malonic acid saturated with oxygen were flowed through the cell. Then neat water was flowed over the sample to remove remaining malonic acid, leaving oxalate on the surface. The difference between the two spectra shown in Fig. 7 is the type of oxygen used in the corresponding experiment; for the top (bottom) spectrum, labeled $^{18}O_2$ (unlabeled O_2) was used. Clearly, in the upper spectrum, some bands are shifted to lower wavenumbers. The band of normal oxalate at 1421 cm^{-1} shifts down to 1400 cm^{-1}, and the broad band at 1633 cm^{-1} shifts down to 1590 cm^{-1}. These bands are associated with C–O vibrations [25], and thus the shifts show that ^{18}O from dissolved oxygen is incorporated into the adsorbed oxalate. Fig. 7 indicates that reactive species formed from oxygen (electron acceptor) can react directly with the adsorbed C_2 species, that is, the carbon-centered radical or the species resulting from it. Interestingly,

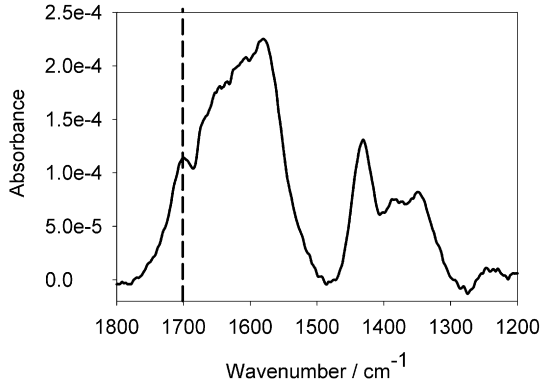

Fig. 8. ATR-IR spectrum obtained while flowing a solution of malonic acid saturated with nitrogen over the TiO_2 sample during illumination. The vertical line indicates the strongest oxalate band.

there was no clear sign in the spectra of ^{18}O-labeled CO_2 (data not shown). We attribute this only in part to a low signal-to-noise ratio. More importantly, oxygen exchange between CO_2 and the TiO_2 surface is possible [39]. Sato showed that oxygen isotope exchange among water, CO_2, and surface hydroxyls readily occurs on TiO_2 even in the dark [40]. This means that the labeled oxygen found in the oxalate (Fig. 7) can be exchanged with normal oxygen once adsorbed CO_2 is formed, and thus the dissolved CO_2 is mostly unlabeled due to the large excess of normal oxygen in the system.

Fig. 8 shows an ATR-IR spectrum recorded while a solution of malonic acid saturated with nitrogen was flowed over the TiO_2 sample during illumination. Fig. 8 reveals that oxalate also can be formed from malonate on illumination in the absence of oxygen. This finding shows that oxygen from a different source than dissolved oxygen (i.e., from water or the TiO_2 surface) also can be incorporated into the oxalate.

Dissolved oxygen not only acts as one possible source of oxygen atoms, but also has a pronounced influence on the reaction rate. Fig. 9 shows the signal at 1700 cm^{-1} associated with the oxalate on the TiO_2 surface as a function of time during one modulation period. In this experiment, the dissolved gas was modulated between N_2 and O_2. The coverage of oxalate is clearly modulated, showing an increase in oxygen and a decrease in nitrogen. The rates of the various reaction steps can be influenced by the dissolved oxygen mainly in two ways. Oxygen acts as an acceptor for the electron of the photogenerated electron–hole pair. The resulting reactive species can directly attack adsorbed molecules, as is suggested by the $^{18}O_2$ experiments (Fig. 7). The acceptance of the electron furthermore leads to an increased lifetime of the photogenerated hole, and thus to an increased reaction rate.

3.5. Mineralization of succinic acid

Fig. 10 shows several ATR-IR spectra related to the mineralization of succinic acid over TiO_2. Trace (a) shows a spectrum of succinic acid adsorbed on TiO_2 in the dark. The two subsequent spectra, (b) and (c), were recorded while succinic acid was flowed over the TiO_2 film during illumination. Spectrum (d) represents the difference between two spectra recorded at

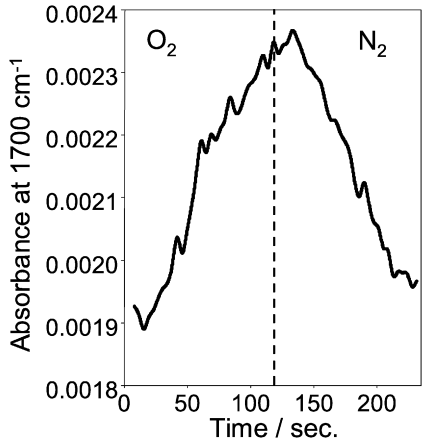

Fig. 9. ATR-IR signal at 1700 cm^{-1} associated with oxalate as a function of time during a modulation experiment ($T = 232$ s). In this experiment a solution of malonic acid (1.5×10^{-4} mol/L) was flowed over the TiO_2 sample during illumination. The stimulation parameter was the dissolved gas, which was O_2 during the first half period and N_2 during the second half period. The vertical line indicates the time at which the dissolved gas was changed from O_2 to N_2.

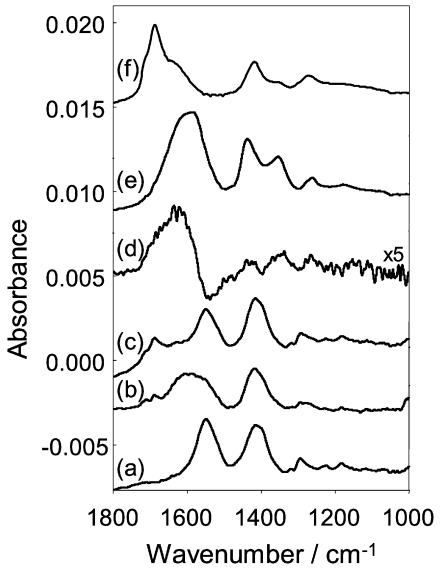

Fig. 10. ATR-IR spectra related to succinic acid mineralization. Spectrum (a) was obtained while flowing succinic acid (1.5×10^{-4} mol/L) over the sample in the dark (for 30 min). Spectra (b) and (c) were measured during illumination, spectrum (b) 11 min and spectrum (c) 37 min after turning the light on. Spectrum (d) represents the spectral differences observed during the first 83 s of illumination. Spectra (e) and (f) are the spectra of adsorbed malonate and oxalate for comparison.

the very beginning of illumination. Finally, the two top traces, (e) and (f), represent the spectra of adsorbed malonate and oxalate on TiO_2 for comparison.

The spectrum of succinic acid adsorbed in the dark from water is characterized by two strong bands at 1550 and 1417 cm^{-1}, which can be assigned to antisymmetric and symmetric COO^- stretching vibrations, respectively. This shows that the molecule exists as succinate on the TiO_2 surface. The spectrum is significantly different from that of malonate on TiO_2. The latter shows two distinct bands for the symmetric COO^- stretching vibration and two bands for the antisymmetric COO^- stretching vibration, whereas the succinate spectrum is characterized by only one band for the symmetric COO^- stretching vibration and one for the antisymmeteric COO^- stretching vibration. This indicates that the two carboxylate groups in the succinate are equivalent. Based on the energy difference Δ between the two carboxylate stretching modes, an adsorption geometry can be proposed [41]. Because Δ is smaller for the adsorbed succinate than for the succinate in solution, chelating and/or bridging coordination of both COO groups is indicated.

On illumination, a broad band centered at around 1600 cm^{-1} is growing in fast [Fig. 10, spectrum (b)] and later becomes weaker again [Fig. 10, spectrum (c)]. Simultaneously, two signals are steadily growing in at 1708 and 1690 cm^{-1}, which can be assigned to oxalate. Note that the oxalate bands reveal a different kinetics from the band at 1600 cm^{-1}. The difference spectrum in Fig. 10, spectrum (d) was recorded at the very beginning of illumination. In this spectrum, the two most prominent bands of succinate appear negative, due to the disappearance of succinate from the surface. Positive bands also are observed associated with species appearing on the surface on illumination. Comparison with the two spectra shown on top in Fig. 10 reveals that these positive bands belong to malonate and oxalate. From the kinetics of appearance and disappearance of these bands, as discussed above, it can be concluded that succinate is transformed to malonate and then to oxalate. Thus, it seems that one dominant pathway for the photocatalytic mineralization of aliphatic dicarboxylic acids on TiO_2 is the consecutive shortening of the hydrocarbon chain by formal CH_2 elimination. Each of these formal steps is initiated by a photo-Kolbe reaction, which results in the elimination of CO_2, and subsequent steps that lead from the carbon-centered radical to a carboxylate.

4. Conclusion

ATR-IR spectroscopy in combination with modulation excitation spectroscopy and isotope labeling was used to study the mineralization of malonic acid over P25 TiO_2 photocatalyst. The enhanced sensitivity achieved by the phase-sensitive detection of periodically varying signals made the detection of dissolved CO_2 possible. From the relative signals of CO_2 and $^{13}CO_2$ observed during the mineralization of selectively labeled malonic acid, it was determined that 50% of the adsorbed malonate was completely converted to CO_2 (via oxalate), whereas 50% of the C_2 intermediates generated after the first photo-Kolbe reaction were desorbed from the surface and washed away without being oxidized. Modulation experiments also revealed the presence of carbonates on the TiO_2 surface during illumination. Experiments in the presence of labeled $^{18}O_2$ showed that the ^{18}O is incorporated into the adsorbed oxalate. On the other hand, oxalate also was formed from malonate on illumination in the absence of dissolved oxygen. This shows that at least two different pathways lead from the carbon-centered radical to the oxalate after the first photo-Kolbe reaction. These pathways are characterized by different oxygen sources, dissolved oxygen and possibly oxygen from water. Dissolved oxygen furthermore influences the rates of the

different reaction steps. It acts as an electron acceptor and accelerates the photocatalytic reactions by preventing electron–hole recombination.

Acknowledgment

Funding was provided by the Swiss National Science Foundation.

References

[1] R. Wang, K. Hashimoto, M. Chikuni, E. Kojima, A. Kitamura, M. Shimohigashi, T. Watanabe, Nature 388 (1997) 431.
[2] R. Asahi, T. Morikawa, T. Ohwaki, K. Aoki, Y. Taga, Science 293 (2001) 269.
[3] M.R. Hoffmann, S.T. Martin, W.Y. Choi, D.W. Bahnemann, Chem. Rev. 95 (1995) 69.
[4] P. Calza, E. Pelizzetti, C. Minero, J. Appl. Electrochem. 35 (2005) 665.
[5] O. Carp, C.L. Huisman, A. Reller, Prog. Solid State Chem. 32 (2004) 33.
[6] N.J. Harrick, Internal Reflection Spectroscopy, Interscience Publishers, New York, 1967.
[7] M.I. Tejedor-Tejedor, E.C. Yost, M.A. Anderson, Langmuir 6 (1990) 979.
[8] S.J. Hug, B. Sulzberger, Langmuir 10 (1994) 3587.
[9] T. Bürgi, R. Wirz, A. Baiker, J. Phys. Chem. B 107 (2003) 6774.
[10] T. Bürgi, A. Baiker, J. Phys. Chem. B 106 (2002) 10649.
[11] S.D. Ebbesen, B.L. Mojet, L. Lefferts, Langmuir 22 (2006) 1079.
[12] G. Mul, G.M. Hamminga, J.A. Moulijn, Vib. Spectrosc. 34 (2004) 109.
[13] I. Ortiz-Hernandez, C. Williams, Langmuir 19 (2003) 2956.
[14] R. He, R.R. Davafa, J.A. Dumesic, J. Phys. Chem. B 109 (2005) 2810.
[15] T. Bürgi, A. Baiker, Adv. Catal. 50 (2006) 228.
[16] D. Ferri, C. Mondelli, F. Krumeich, A. Baiker, J. Phys. Chem. B 110 (2006) 22982.
[17] R. Nakamura, A. Imanishi, K. Murakoshi, Y. Nakato, J. Am. Chem. Soc. 125 (2003) 7443.
[18] R. Nakamura, Y. Nakato, J. Am. Chem. Soc. 126 (2004) 1290.
[19] D.S. Warren, A.J. McQuillan, J. Phys. Chem. B 108 (2004) 19373.
[20] J.M. Kesselman-Truttmann, S.J. Hug, Environ. Sci. Technol. 33 (1999) 3171.
[21] G.N. Ekström, A.J. McQuillan, J. Phys. Chem. B 103 (1999) 10562.
[22] P.Z. Araujo, C.B. Mendive, L.A.G. Rodenas, P.J. Morando, A.E. Regazzoni, M.A. Blesa, D. Bahnemann, Colloids Surf. A Physicochem. Eng. Aspects 265 (2005) 73.
[23] C.B. Mendive, D.W. Bahnemann, M.A. Blesa, Catal. Today 101 (2005) 237.
[24] I. Dolamic, T. Bürgi, J. Phys. Chem. B 110 (2006) 14898.
[25] C.B. Mendive, T. Bredow, M.A. Blesa, D.W. Bahnemann, Phys. Chem. Chem. Phys. 8 (2006) 3232.
[26] D. Baurecht, U.P. Fringeli, Rev. Sci. Instrum. 72 (2001) 3782.
[27] A. Gisler, T. Bürgi, A. Baiker, J. Catal. 222 (2004) 461.
[28] T. Bürgi, M. Bieri, J. Phys. Chem. B 108 (2004) 13364.
[29] A. Urakawa, R. Wirz, T. Bürgi, A. Baiker, J. Phys. Chem. B 107 (2003) 13061.
[30] S. Hug, D. Bahnemann, J. Electron Spectrosc. Relat. Phenom. 150 (2006) 208.
[31] T. Sakata, T. Kawai, K. Hashimoto, J. Phys. Chem. 88 (1984) 2344.
[32] B. Kraeutler, A.J. Bard, J. Am. Chem. Soc. 99 (1977) 7729.
[33] M. Falk, A.G. Miller, Vib. Spectrosc. 4 (1992) 105.
[34] F.P. Rotzinger, J.M. Kesselman-Truttmann, S. Hug, V. Shklover, M. Grätzel, J. Phys. Chem. B 108 (2004) 5004.
[35] Physical and Engineering Data, January 1978 ed., Shell Internationale Petroleum Maatschappij BV, The Hague, 1978.
[36] W. Gu, C.P. Tripp, Langmuir 22 (2006) 5748.
[37] A. Davidov, Molecular Spectroscopy of Oxide Catalyst Surfaces, Wiley, West Sussex, 2003.
[38] N. Serpone, Y. Nakaoka, J. Nishino, Y. Nosaka, in: D.F. Ollis, H. Al-Ekabi (Eds.), Photocatalytic Purification and Treatment of Water and Air, Elsevier, Amsterdam, 1993.
[39] H. Hattori, Chem. Rev. 95 (1995) 537.
[40] S. Sato, J. Chem. Phys. 91 (1987) 2895.
[41] G.B. Deacon, R.J. Phillips, Coord. Chem. Rev. 33 (1980) 227.